

# A Comprehensive Analysis of Near-Contact Photobiomodulation Therapy in the Host-Bacteria Interaction Model Using 3D-Printed Modular LED Platform

Hye-Eun Kim, Sayemul Islam, Moonchul Park, Albert Kim,\* and Geelsu Hwang\*

One well-studied bacterial factor recognized by the host immune system is lipopolysaccharides (LPS) that stimulate host cells, resulting in cell inflammation. Although photobiomodulation (PBM) therapy demonstrates its potency on anti-inflammatory activity, the complete mechanism of action in the host-bacteria interaction model is still elusive. In addition, many studies were performed regarding a distance between the light source and biological sample (non-contact therapy) that may result in disparate reports on the efficacy of PBM therapy. Thus, it is critical to clearly understand the effect of this approach to maximize efficacy and minimize side effects. Here, a custom-built light-emitting diode (LED) platform that mimics near-contact therapy is developed. The effect and mechanism of PBM therapy on epithelial cells in response to LPS is systematically investigated under various conditions (wavelength, irradiation-time, pulse-frequency). The data show that the irradiation of near-infrared (NIR-LED) significantly improves the viability of inflamed cells. It reveals that NIR-LED inhibits the production of reactive oxygen species by regulating the Nox4-NF-κB pathway. Interestingly, however, high-pulse frequency stimulus causes the collapse of the mitochondrial membrane potential ( $\Delta \Psi m$ ) of cells, resulting in cell death. These results suggest that the optimized "PBM condition" is critical to assist the healthy immune system of the host against bacterial invasion.

#### 1. Introduction

A myriad of microorganisms exists in close proximity to tissues in the human body, while a highly efficient innate host defense system constantly monitors the status of microbial colonization, and prevents their intrusion by forming a protective

Dr. H. E. Kim, Prof. G. Hwang
Department of Preventive and Restorative Sciences
Center for Innovation & Precision Dentistry
School of Dental Medicine
University of Pennsylvania
Philadelphia, PA 19104, USA
E-mail: geelsuh@upenn.edu
S. Islam, M. Park, Prof. A. Kim
Department of Electrical and Computer Engineering
Temple University
Philadelphia, PA 19122, USA
E-mail: albertkim@temple.edu
The ORCID identification number(s) for the author(s) of this article

can be found under https://doi.org/10.1002/adbi.201900227.

DOI: 10.1002/adbi.201900227

barrier.[1] The penetration of this barrier by bacterial invasion results in an inflammation, which is an essential response of the host upon infection or tissue invasion.<sup>[2]</sup> In most cases, the process leads to the elimination of the intrusive microorganisms without significant signs of inflammation. However, it can be further developed to pathological processes that may culminate in severe conditions such as multiple organ failure and even death.[2] Since initial and mild cell inflammation can be reversible to a healthy condition, recovering cell inflammation in the early stage is critical for the prevention of further inflammatory diseases.

Lipopolysaccharides (LPS)-induced inflammation in human alveolar basal epithelial cells (A549) is a well-established in vitro model to observe host–bacteria interactions.<sup>[3–7]</sup> LPS is the major virulent component of the outer membrane of gram-negative bacteria that stimulates host cells and induces cell inflammation.<sup>[8]</sup> LPS can rapidly trigger an intracellular signaling pathway, resulting in the release of proinflammatory mediators such as

the production of cytokines.<sup>[8,9]</sup> For example, LPS is recognized by Toll-like receptor 4 (TLR4) that plays a role in pathogen recognition and activation of innate immunity. When LPS binds to TLR4, it results in boosting of the intracellular signal via Myeloid differentiation primary response 88 (MyD88) and subsequently phosphorylates nuclear factor kappa-light-chain-enhancer of activated B cells (NF- $\kappa$ B). The phosphorylated NF- $\kappa$ B (p-NF- $\kappa$ B) is then translocated into the nucleus where it binds to promoter regions of target genes.<sup>[9]</sup> Meanwhile, nicotinamide adenine dinucleotide phosphate (NADPH) oxidase 4 (Nox4) can interact directly with the cytoplasmic tail of TLR4, contributing to NF-κB activation.[10,11] NF-kB is an important regulator of the immune system, and activation of NF-kB increases the transcription of genes involved in innate immune and inflammatory responses.<sup>[12]</sup> Therefore, determining the TLR4/Nox4-MyD88-NF-κB signaling pathway is important for understanding the mechanism of cell inflammation as well as developing a therapeutic approach to prevent cell inflammation against bacterial invasion.

As a therapeutic approach capable of inhibition of promoting tissue healing and reducing cell inflammation, <sup>[13,14]</sup> the photobiomodulation (PBM) therapy has been highlighted;

www.adv-biosys.com

however, it has also been debated without a consensus of optimized therapeutic parameters.<sup>[15]</sup> Several reports showed varied physiological effects of PBM therapy depending on a specific range of wavelength, energy density, pulse frequency, and target disease models. For example, Kolb-Bachofen and coworkers found that light at wavelengths of 632–940 nm has no effect, but irradiation with a blue light at 412–426 nm exerts toxic effects at high fluences (>500 J cm<sup>-2</sup>) on human keratinocytes.<sup>[16]</sup> On the other hand, many reports showed red-to-infrared wavelength (620–1200 nm) enhances cell proliferation and anti-inflammation on human keratinocytes.<sup>[17,18]</sup> In spite of potent biological functions of PBM therapy on promoting tissue healing and reducing inflammation, it is as yet unclear its complete mechanism of action on cells in response to LPS-induced inflammation in the context of host–bacteria interaction.

Since the PBM therapy may have different optimal "dose" and exceeding this may alter its biological function from recovering of cells to killing as in photodynamic therapy, a thorough understanding of its effects depending on operating conditions, such as wavelength, exposure time, pulse frequency, and energy density of light-emitting diode (LED), are warranted. In addition, there are many commercial wearable phototherapy devices in near-contact for clinical purposes such as the treatment of joint inflammation and edema.[19] However, these were not carefully investigated because most of the in vitro PBM therapy studies were performed in a distance between the light source and biological sample with high energy density; the energy density received at the level of biological samples is inversely proportional to the square of the distance, the emission angle at the distance may change the effective light irradiance, and the ambient light could deviate the efficacy. In addition, the use of high energy can cause excessive heat accumulation and tissue heating that may negatively impact outcomes.<sup>[20]</sup>

In this study, we developed a custom-built LED platform that uses low energy that can mimic near-contact therapy to precisely evaluate PBM therapy in vitro and systematically investigated its efficacy on host-bacteria interaction using A549 cells and bacterial LPS as model organisms. We also attempted to find an optimized PBM dose by irradiating LEDs with four different distinctive wavelengths ( $\lambda = 465$  nm [blue, B], 575 nm [green, G], 615 nm [red, R], and 880 nm [near-infrared, NIR]), energy density (mW cm<sup>-2</sup>), and pulse frequency (5 or 500 Hz). Our data showed that cell viability was significantly improved when the cells were exposed to R or NIR LEDs (without LPS stimulus), proportional to energy density (up to 4.50 J cm<sup>-2</sup>), compared with cells without LED irradiations (i.e., control group). G LED did not show any effect regardless of exposure time, while B LED decreased cell viability significantly proportional to exposure time. Interestingly, the NIR irradiation showed better efficacy than the R irradiation, and only the NIR irradiation recovered the inflamed cells and improved their viability significantly (≈20%) higher than that of the control group (no LPS, no light irradiation). However, the high pulse frequency stimulus caused the collapse of the mitochondrial membrane potential (ΔΨm) of cells, resulting in subsequent cell death. Importantly, the signaling pathway data revealed that the major mechanism of action of PBM therapy is deeply associated with the inhibition of reactive oxygen species (ROS) production and Nox4 expression level.

## 2. Results

#### 2.1. Customization and Characterization of LED Platform

To investigate the near-contact PBM therapy and its optimal operation conditions for efficacious effect, a high-throughput modular LED platform was designed (Figure 1). A disc that has a size equivalent to a single well of the 24-well cell plate (d = 15.4 mm, t = 2 mm) was 3D printed (Form 2, Formlabs, Inc.). The disc also incorporated a small slot (dimension of  $5 \times$  $2 \times 1 \text{ mm}^3$ ) in the middle to accommodate a miniaturized LED circuit (Figure 1A). Four different LED components with distinctive wavelengths were selected ( $\lambda = 465$  [B], 575 [G], 615 [R], and 880 nm [NIR]) (see Experimental Section). The LED platform was completed by placing the LED discs inside the bottom of a custom-designed black box that can house a cell plate while blocking ambient light (Figure 1B, a lid not shown). During the placement, the LED discs were aligned with an individual well of the cell plate that sits on top, making direct contact between the cell plate and LED discs (Figure 1C).

The light irradiance and the emission angle by the LED platform were determined to be uniform across all wavelengths. We have set the light irradiance at the level of cells to 0.8 mW cm<sup>-2</sup>, which exhibited minimal thermal effects (<1.1 °C) (measured ≈3 weeks; Figure S1, Supporting Information). Based on the light irradiance, the input driving voltage was regulated individually for each wavelength. While the fabricated LED disc was placed on an optic table, the light irradiance was measured using a photodetector (FDS1010, Thorlabs) at the same height that the cell plate sits (the distance between the LED disc and the bottom of cell plate was 2.3 mm) (Figure 1D). The voltages that were able to irradiate 0.8 mW cm<sup>-2</sup> were  $V_{NIR} = 2 \text{ V}$ ,  $V_{R} = 5.94 \text{ V}$ ,  $V_{G} = 4.3 \text{ V}$ , and  $V_{R} = 2.85 \text{ V}$ . Since the light emission angle was predetermined by a manufacturer, we have selected the LEDs that have the emission angle of 120° or larger for uniform light coverage on cells. The light energy density that the cells received was analyzed based on the measured light irradiance up to 120 min (same exposure time to in vitro experiments); the energy densities were almost identical (e.g., average energy density of ≈6.00 J cm<sup>-2</sup> when irradiated for 120 min) (Figure 1E; Table S1, Supporting Information).

For the pulse frequency PBM therapy study, a LED driving circuitry capable of modulating frequency was separately designed (Figure 1F). The LED driving circuit consists of two to four individually tuned timer circuits and nine amplifier circuits to simultaneously operate multiple LEDs with three different driving voltages and frequencies. (Figure 1G shows three-timer circuits and nine amplifier circuits). Each timer circuit was tuned to generate square waves whose frequency can be adjusted (5 or 500 Hz) with a 50% duty cycle. Lastly, the voltage output of the timer circuit was amplified to a previously determined driving voltage for each LED using an amplifier.

# 2.2. Effects of LED Irradiations for Cell Proliferation on A549 cells

To comprehensively analyze the effect of PBM therapy on cell proliferation, especially recovery from bacterial invasion,

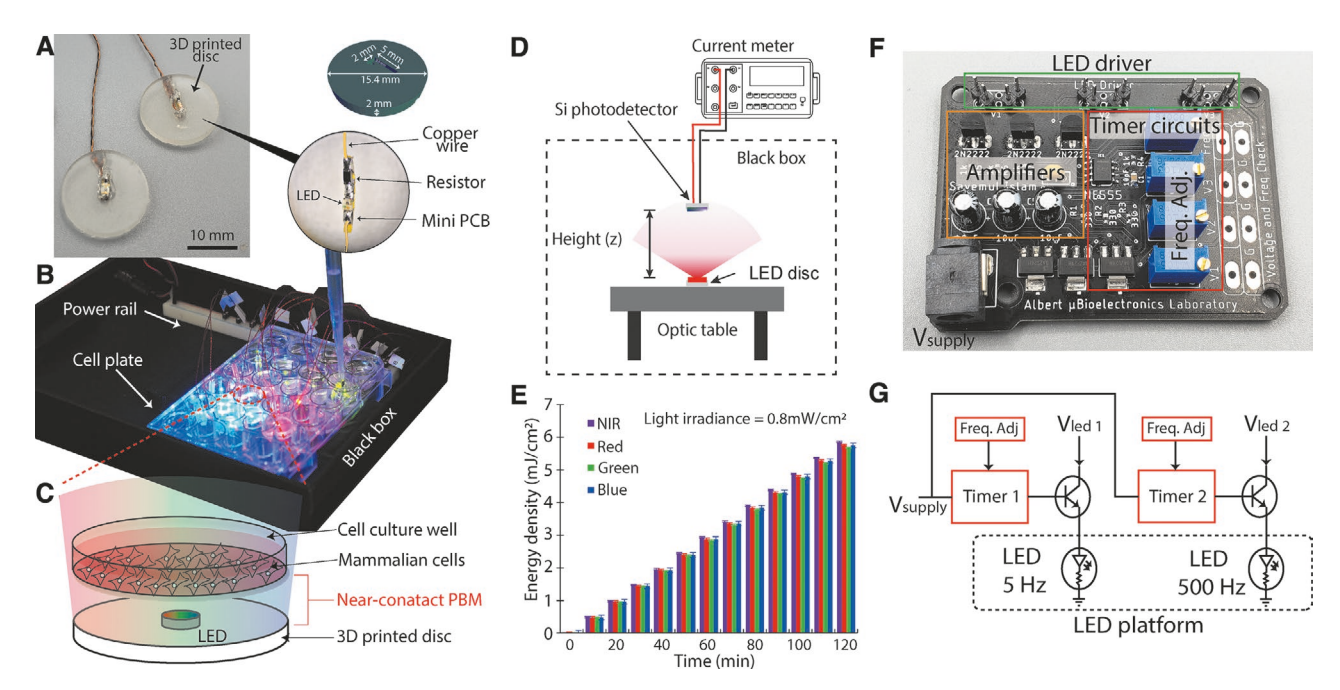


Figure 1. Schematic view of a custom-built LED device for near-contact PBM therapy. A) A framework of LED disc that holds a LED and a current limiting resistor inside. B) An LED platform consists of a black box, multiple LED discs, and an external power (not shown). C) Schematic diagram of near-contact PBM therapy: an LED disc directly contact to the bottom of cell culture plate containing mammalian cells. D) A setup of LED light irradiance measurement. E) Energy densities of LEDs depending on the wavelength and irradiation time. F) An external LED driving circuit for pulse frequency PBM therapy. G) A diagram of a LED driving circuit.

we investigated various PBM therapy parameters (e.g., wavelength, exposure time, light energy density, and light irradiance frequency) on A549 cells. First, we prepared A549 cells by incubating for 24 h. As shown in Figure 2, cell viability was increased over time in the presence of F-12K medium (Kaighn's modification of Ham's F-12). Then, we irradiated LEDs using various light parameters with a range of wavelength (from  $\lambda = 465$  [B] to 880 nm [NIR]) and energy density (up to  $\approx 6.00$ J cm<sup>-2</sup>) on 24 h pre-cultured intact A549 cells (see Experimental Section for the details). The data showed that the higher wavelength (R, 615 nm and NIR, 880 nm) irradiations increased cell viability in proportional to exposure time (up to  $\approx 4.50 \text{ J cm}^{-2}$ ). Interestingly, R irradiation at ≈6.00 J cm<sup>-2</sup> energy density reduced the cell viability significantly as compared to 90 min exposure, while the same energy density of NIR did not affect the cell viability negatively. By contrast, strong photocytotoxicity was observed when the cells were exposed to lower wavelength light (B, 465 nm), showing a linear reduction of cell viability in a time-dependent manner. However, green light irradiation (G, 575 nm) did not affect A549 cell proliferation regardless of exposure time.

#### 2.3. Effect of Bacterial LPS on A549 Cells

To determine LPS treatment condition for mild inflammation of cells without severe death, we exposed pre-cultured A549 cells to various LPS concentration with a range of 0– $100 \mu g mL^{-1}$  for 24 h (**Figure 3**). The cell viability was decreased in proportional to LPS concentration (Figure 3A). Exposure of cells to  $10 \mu g mL^{-1}$ 

reduced cell viability slightly (p > 0.05), while higher than 20 µg mL<sup>-1</sup> of LPS significantly lower the cell viability (vs non-LPS-treated cells). The reduction of cell viability may increase the level of proinflammatory markers.<sup>[21]</sup> Thus, we examined the effect of bacterial LPS on the production of cytokines, such

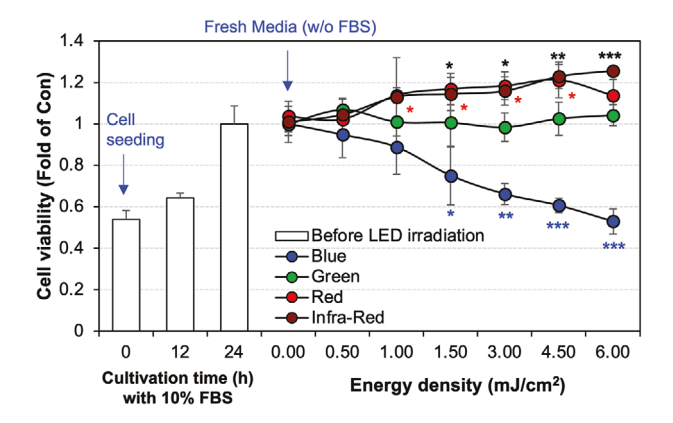


**Figure 2.** Effect of LED irradiations on cell viability of A549 cells. Cell viability was examined under a range of energy density (up to  $\approx$ 6.00 J cm<sup>-2</sup>) with a range of wavelength (Blue: 465 nm, Green: 575 nm, Red: 615 nm, NIR: 880 nm) with 0% F-12K medium. Cell viabilities under PBM therapy were normalized by the control group (no PBM therapy). Red or NIR irradiations increased cell viability in proportional to energy density (up to  $\approx$ 4.50 J cm<sup>-2</sup>), while blue irradiation exhibited a linear reduction of cell viability in a time-dependent manner and green irradiation did not affect the viability of A549 cells, regardless of energy density. Error bars represent SD;  $n \ge 4$ ; p-value was determined using a two-tailed t-test. \*p < 0.05, \*\*p < 0.01, \*\*\*p < 0.001.

www.advancedsciencenews.com www.adv-biosys.com

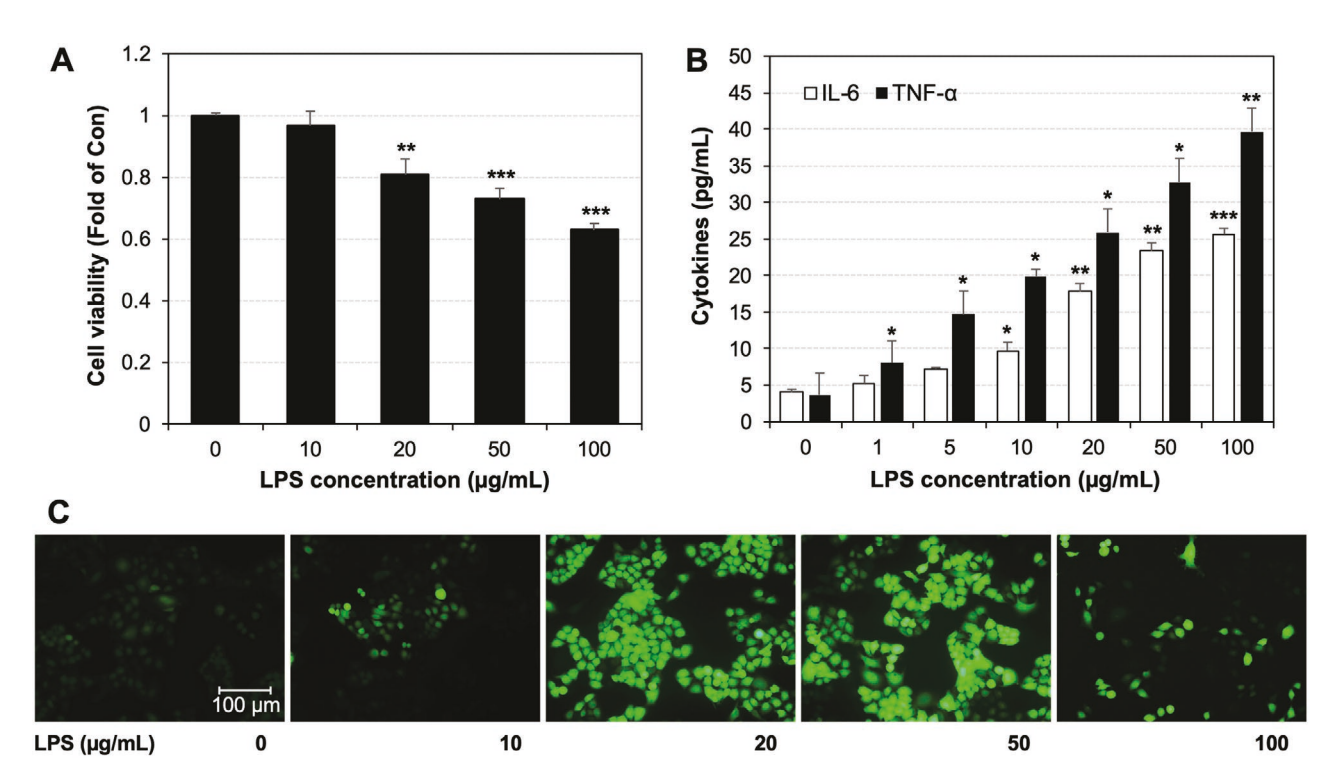


Figure 3. Effect of LPS treatment on A549 cells. A) Normalized cell viability depending on the concentration of LPS: A549 cells were treated with 1–100 μg mL<sup>-1</sup> LPS for 24 h to analyze the viability of cells via MTT assay. Over 20 μg mL<sup>-1</sup> of LPS reduced the cell viability significantly compared to control. B) Amount of produced cytokines by LPS stimuli: expression levels of IL-6 and TNF-α were significantly higher than control when LPS is over 1 and 5 μg mL<sup>-1</sup>, respectively. C) fluorescence images of LPS-treated cells: green fluorescence indicates production of intracellular ROS, showing the highest signal at 20 μg mL<sup>-1</sup> of LPS. Reduction of ROS signal was observed when LPS is higher than 50 μg mL<sup>-1</sup>, possibly due to severe cell death, resulting in less production of ROS. Error bars represent SD;  $n \ge 4$ ; p-value was determined using a two-tailed t-test. \*p < 0.05, \*\*p < 0.01, \*\*\*p < 0.001.

as interleukin 6 (IL-6) and tumor necrosis factor- $\alpha$  (TNF- $\alpha$ ). The level of both IL-6 and TNF- $\alpha$  started to increase significantly at the concentration of LPS 5  $\mu g\ mL^{-1}$  (Figure 3B), while it did not affect the cell viability up to LPS 10 μg mL<sup>-1</sup>, indicating the self-recovery ability of A549 cells against mild inflammation. Since LPS is known to stimulate host cells to release ROS,<sup>[22]</sup> we investigated the production of ROS by LPS. To assess the level of intracellular ROS after LPS exposure, the production of intracellular ROS levels was measured using dichlorofluorescin diacetate (DCF-DA) fluorescence.<sup>[23]</sup> In the presence of intracellular esterases and oxidizing molecules such as O<sub>2</sub>, H<sub>2</sub>DCF-DA is converted to the highly fluorescent DCF. Green fluorescent indicates the produced ROS, showing the highest level of ROS signal at LPS 20 μg mL<sup>-1</sup> (Figure 3C; Figure S2, Supporting Information). The reduction of ROS signal was observed when LPS was higher than 50 µg mL<sup>-1</sup>, possibly due to severe cell death, resulting in less production of ROS.

# 2.4. Effect of PBM Therapy on A549 Cells against LPS-Induced Inflammation

Based on the results of LED irradiance and bacterial LPS on A549 cells, we further investigated the efficacy of PBM therapy on LPS-inflamed cell under two parameters: 1)  $\approx$ 4.50 J cm<sup>-2</sup> energy density because it showed the highest

viability of intact cell when R or NIR was irradiated, and 2) 20 µg mL<sup>-1</sup> of LPS due to inflammation initiation without severe cell death (Figure 4). First, we determined how effectively PBM therapy can improve the viability of LPS-inflamed A549 cells. We did not observe the improvement of cell viability under B or G irradiation, rather these conditions substantially lowered the cell viability when exposed to LPS (vs B or G without LPS treatment) (Figure 4A). However, irradiation of R maintained the viability of inflamed cells similar level to that of intact cells (i.e., control; no LPS, no LEDs), while it did not reach the level of viability of R without LPS. Interestingly, there were no significant differences in cell viability when exposed to NIR (regardless of LPS treatment), indicating its strong anti-inflammatory activity against LPS stimulus. Then, we determined the level of proinflammatory markers showing that R or NIR irradiation significantly inhibits the production of IL-6 and TNF-lpha (vs cells with LPS but no light irradiation) (Figure 4B,C). Particularly, NIR exposure reduced the production of both IL-6 and TNF- $\alpha$  approximately threefold compared to control. Finally, we investigated the ROS production in these conditions. In the absence of LPS, all the conditions showed a similar level of ROS production regardless of irradiation. LPS substantially induced the ROS production; however, R irradiation decreased its level significantly and NIR even further inhibited the ROS production, comparable to that of no LPS condition (Figure 4D).

www.adv-biosys.com

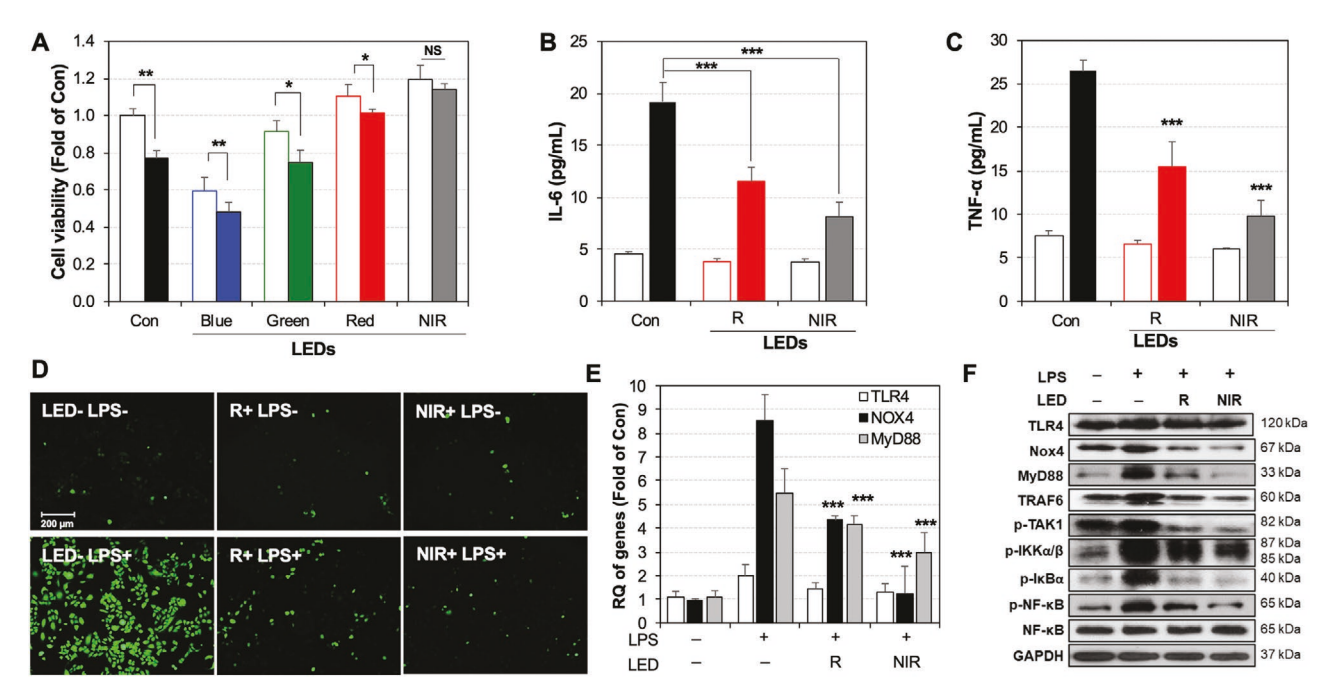


Figure 4. Effect of red (R) and NIR irradiations on inflamed cells by LPS. A) Normalized viabilities of cells and expression level of proinflammatory markers, B) IL-6 and C) TNF- $\alpha$ , with or without LPS inflammation (20 μg mL<sup>-1</sup>) in the absence or presence of LED irradiations (90 min): R irradiation maintained the viability of inflamed cells to that of control, while NIR irradiation significantly improved the cell viability, regardless of LPS treatment. NIR irradiation reduced the expression level of IL-6 or TNF- $\alpha$  more efficiently than R irradiation. Empty columns indicate without LPS condition and the filled columns indicate with LPS inflammation. D) fluorescence images of cells with or without LPS inflammation (20 μg mL<sup>-1</sup>) in the absence or presence of R or NIR irradiations: either R or NIR irradiation reduced the production of ROS significantly compared to inflamed cells without LED irradiation (LED- LPS+). E) qRT-PCR analyses of TLR4, Nox4, and MyD88: NIR irradiation reduced the expression level of TLR4 or MyD88 more efficiently than R irradiation. (F) Western blotting analyses of TLR4, Nox4, MyD88, TRAF6, p-TAK1, p-IKKα/ $\beta$ , p-IκB $\alpha$ , NF-κB, and p-NF-κB: GAPDH was used as a loading control. Error bars represent SD;  $n \ge 4$ ; p-value was determined using a two-tailed t-test. NS: not significant. \*tp < 0.05, \*\*tp < 0.01, \*\*\*tp < 0.001.

# 2.5. Effect of R or NIR Irradiation on Signaling (Nox4-MyD88-NF-κΒ) Pathway of the LPS-Inflamed Cell

LPS is recognized by TLR4 and it can trigger inflammatory responses via NF-kB activation.[10] Nox4 also can interact with the cytoplasmic tail of TLR4, by coupling with the COOHterminal region of Nox4 in response to LPS, contributing to NF-κB activation.<sup>[24,25]</sup> To determine the TLR4-related pathways of our PBM therapy on anti-inflammatory activity against LPS, we performed qRT-PCR (Figure 4E) and Western blotting assays (Figure 4F; Figure S3, Supporting Information). The data showed that the mRNA and protein expression levels of TLR4 were slightly increased when the cells were exposed to LPS (20 µg mL<sup>-1</sup>) but these expression levels were reduced to those of control under R or NIR therapy at  $\approx 4.50$  J cm<sup>-2</sup>. In contrast, expression levels of Nox4, MyD88, tumor necrosis factor receptor associated factor 6 (TRAF6), p-transforming growth factor beta-activated kinase 1 (p-TAK1), p-IkB kinase (IKK) complex  $\alpha/\beta$  (p-IKK $\alpha/\beta$ ), p-nuclear factor of kappa light polypeptide gene enhancer in B-cells inhibitor  $\alpha$  (p-I $\kappa$ B $\alpha$ ), and p-NF- $\kappa$ B were significantly increased by LPS stimulus, while R or NIR treatment significantly reduced the expression levels of those (Figure 4E,F; Figure S3, Supporting Information). These results suggest that the irradiation of R or NIR can inhibit inflammation by interfering ROS production through the Nox4/MyD88/ NF-κB pathway (Figure S4, Supporting Information).

# 2.6. Effect of Pulse Frequency of R or NIR Irradiation on In Vitro Host-Bacteria Model

It has been reported that pulsed wave (PW) light therapy can be more effective than continuous wave (CW) light therapy in some biological systems. [26-28] To compare the efficacy of PBM therapy on anti-inflammation activity in the LPS involved host-bacteria interaction model, we examined the cell viability and cytokine productions under low or high pulse frequency conditions (5 or 500 Hz; Figure 5). The data showed that in the absence of LPS, both R and NIR irradiations incrementally increased the cell viability according to the increase of energy density (hollow symbols in Figure 5A,B). Interesting results were observed under the LPS-induced inflamed condition; cell viability increased under R irradiation at a frequency of 5 Hz (R-PW<sub>5</sub>), while R irradiation at a frequency of 500 Hz (R-PW<sub>500</sub>) decreased cell viability dramatically when higher than 0.75 J cm<sup>-2</sup> energy density applied (filled symbols in Figure 5A). Pulsed NIR irradiation (NIR-PW<sub>5</sub> or NIR-PW<sub>500</sub>) increased the viability of LPS-inflamed cells; however, recovering of cell viability by NIR-PW500 irradiation was significantly retarded compared to those of NIR-PW5 irradiations, although it did not show a reduction of cell viability that was observed from R-PW<sub>500</sub> (filled symbols in Figure 5B). We also tested the effect of extremely low energy densities with frequencies (lower than 0.25 J cm<sup>-2</sup>); the data revealed that irradiation at 0.03 J cm<sup>-2</sup> barely affected the cell viability,

www.adv-biosys.com

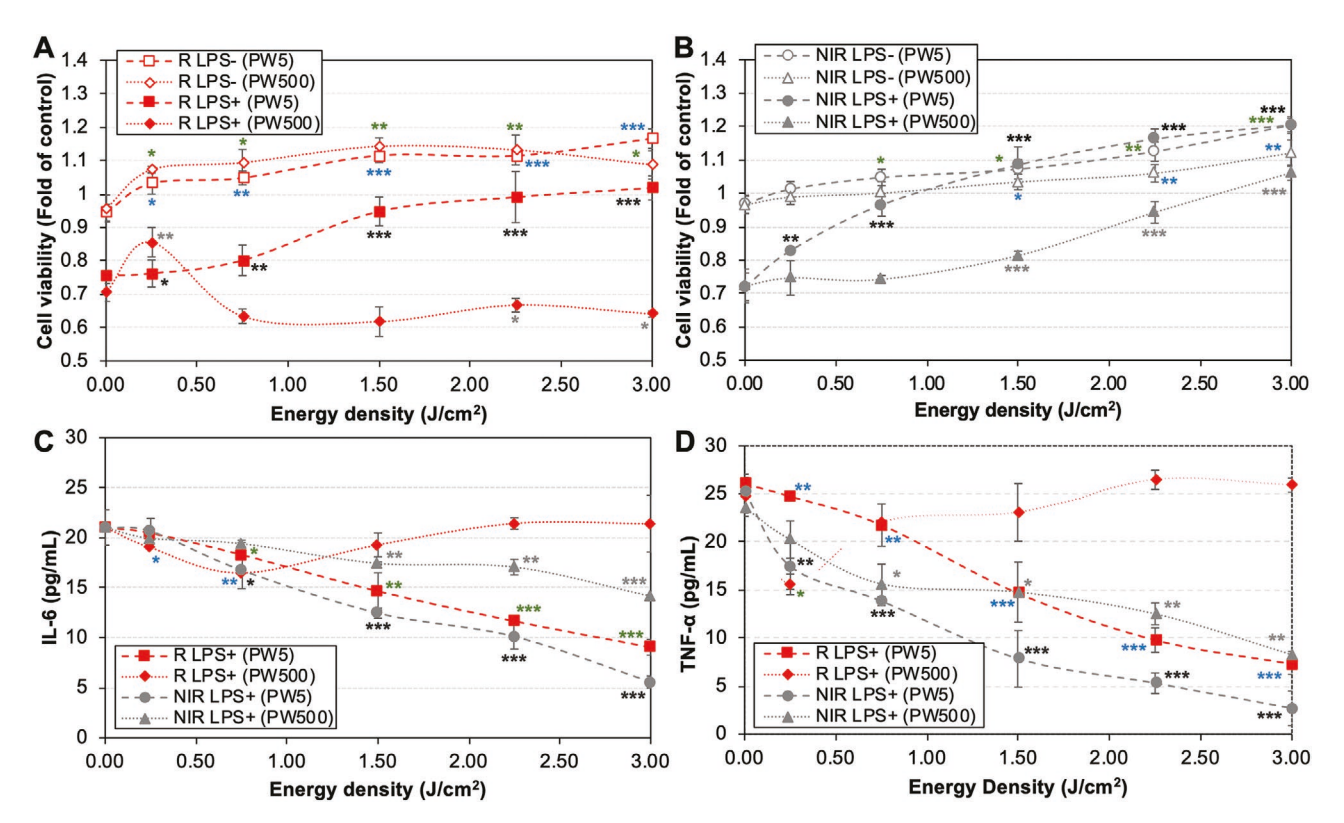


Figure 5. Effect of pulse frequency on cell viability and cell inflammation. Normalized viability of cells with or without LPS inflammation depending on the PW frequencies of A) R and B) NIR irradiations: In general, R and NIR irradiations increased the cell viability in proportional to energy density other than R-PW<sub>500</sub> showing dramatic reduction of cell viability when higher than 0.75 J cm<sup>-2</sup> was applied. The expression level of C) IL-6 and D) TNF-α with or without LPS inflammation depending on the PW frequencies of R and NIR irradiations: The effect of PW irradiation on cell viability is in accordance with the level of inflammation markers, showing that IL-6 and TNF-α were reversely proportional to cell viability. Error bars represent SD;  $n \ge 4$ ; p-value was determined using a two-tailed t-test. \*p < 0.05, \*\*p < 0.001.

while irradiation at 0.13 J cm $^{-2}$  slightly increased the cell viability (Figure S5, Supporting Information). Next, we assessed the level of inflammation markers, IL-6 (Figure 5C) and TNF- $\alpha$  (Figure 5D), under PW conditions. The effect on cell viability by PW irradiation accorded with the effect on the levels of inflammation markers, showing that IL-6 and TNF- $\alpha$  were reversely proportional to cell viability (Figure 5C,D). Interestingly, under the range of energy density between 1.50 and 3.00 J cm $^{-2}$ , R-PW<sub>5</sub> exhibited a similar effect to R-CW, while NIR-PW<sub>5</sub> showed significantly better effect compared to NIR-CW when cells were exposed to LPS (Figures S5, Supporting Information).

Since excessive mitochondrial activation can induce its apoptosis,  $^{[29]}$  we measured the levels of ROS production and mitochondria membrane potential ( $\Delta\Psi$ m) to investigate this unexpected by-effects of PW500 (Figure 6). The carbocyanine fluorescent probe, 5,5′,6,6′-tetrachloro-1,1′3,3′-tetrathylbenzimidazolyl-carbocyanine iodide (JC-1), is a popular fluorochrome for assessing changes in  $\Delta\Psi$ m in mammalian cells, which shows different patterns depending on the level of  $\Delta\Psi$ m: forming a monomeric green-emitting aggregate when  $\Delta\Psi$ m is low (<80–100 mV) while forming a red-emitting aggregate when  $\Delta\Psi$ m is high (>190 mV).  $^{[30]}$  As shown in Figure 6, untreated control displayed no signs of ROS generation and showed large red fluorescing JC-1 aggregates (96.93%). The protonophore, carbonyl cyanide m-chlorophenyl hydrazone

(CCCP), inhibits mitochondrial function by uncoupling oxidative phosphorylation and it has been used as a positive control for cells stained with JC-1.[31] As expected, the green fluorescence was significantly increased when cells were treated with the uncoupler CCCP-positive control (97.8%) or inflamed by LPS (31.08%), indicating decreased ΔΨm and increased apoptosis. Interestingly, we also observed a significant increase of JC-1 green signal when the inflamed cells were exposed to R-PW<sub>500</sub> irradiation (41.47%), compared to R-PW<sub>5</sub> condition (Figure 6A; Figure S6, Supporting Information). However, NIR irradiated cells (all conditions) exhibited significantly higher ΔΨm compared to no irradiation or R-PW<sub>500</sub>, which are consistent with the result of viability assay (Figure 4A) and the DCF-DA results for ROS generation (Figure 4D and 6B). Altogether, the data revealed that low PW frequency irradiation could more effectively scavenge ROS generated by LPS stimulus, while high PW frequency was significantly less efficient to inhibit ROS generation, particularly for R-PW<sub>500</sub> condition.

## 3. Discussion

PBM therapy (or low-level light therapy) has a long history and is a rapidly growing approach to treating a wide range of diseases and disorders that afflict humanity.<sup>[32–34]</sup> Although many

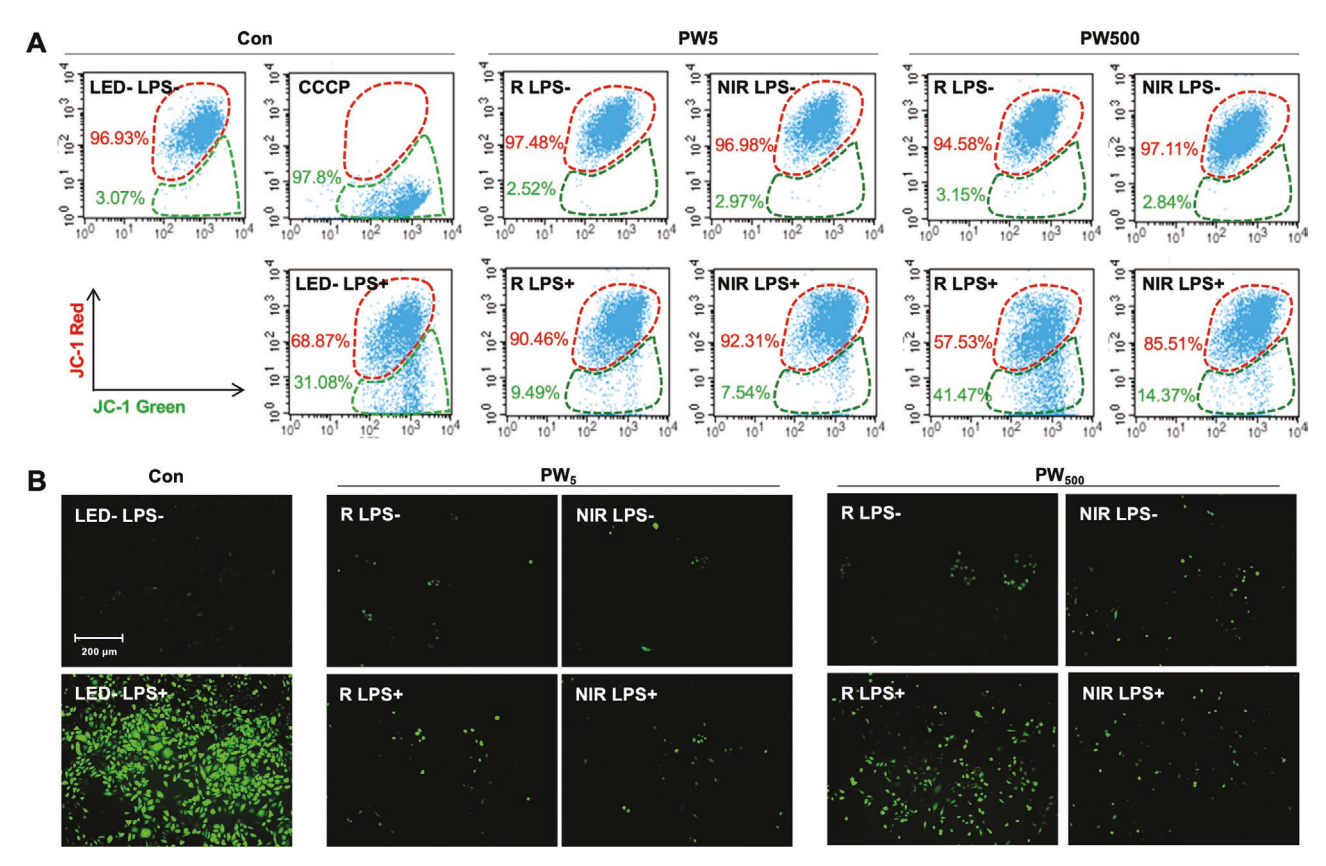


Figure 6. Effect of pulse frequency on mitochondrial membrane potential and ROS generation. A) Map of  $\Delta \Psi m$  in A549 cells with or without LPS inflammation depending on the PW frequencies of R and NIR irradiations: Green fluorescence signal was significantly increased under R-PW<sub>500</sub> condition compared to the untreated control; it shows higher signal intensity than that of LPS without any irradiations. B) Fluorescence images of LPS-treated cells depending on the PW frequencies of R and NIR irradiations: R-PW<sub>500</sub> condition showed significantly higher signal than other conditions, indicating significant production of ROS.

efforts have been made to investigate the effect of PBM therapy and to identify their chromophores and signaling pathways in mammalian cells, [35,36] its basic molecular and cellular mechanism of action is still elusive, particularly in host–bacteria interaction models. Here, we used A549 cell (a model host organism) and *Pseudomonas aeruginosa* LPS (a model inflammatory stimulus) to systematically investigate the efficacy of PBM therapy on anti-inflammatory activity and its underlying mechanism as a model host–bacteria interaction. To the best of our knowledge, the report of optimizing the PBM therapy parameters using the near-contact device in the study of host–bacteria interaction models using A549 cell and *P. aeruginosa* LPS does not yet exist.

Although there are many commercially available wearable phototherapy devices in near-direct skin contact, [19] most of in vitro PBM therapy studies were performed in a distance between the light and biological samples. [17] Since energy density is drastically reduced in proportional to the square of the distance between the light source and target biological sample, operation conditions in those studies may not be relevant to the near-contact PBM therapy. Furthermore, light irradiation at a distance avoids testing of multiple conditions simultaneously due to the wide emission angle. To address these issues, we performed all PBM therapy using the custom-built near-contact

LED platform via 3D printing technology. The modular design of the LED disc allows versatility as the 3D printer can scale up or down the design depending on the type of cell plate. For example, the current design can scale up by 44% for the sixwell cell plate or 28% scaling down for the 48-well cell plate. By incorporating the LED in the middle of the disc and its nearcontact, the LED platform enabled high-throughput screening; it allows to perform multiple experiments with different experimental groups (e.g., different wavelengths) simultaneously without interfering the adjacent wells due to minimized refraction and focused irradiation of light. The optical properties (i.e., light irradiance, light emission angle, and light energy density) were also measured and analyzed at the level of cells, which could reveal the efficacy of the PBM therapy more precisely. Finally, this system requires significantly less power to drive the light source (LED) to achieve the same energy density on cells, thereby reducing negative thermal effects and eliminating the need for a cooling system.

By testing various operating conditions such as wavelength (blue to NIR), energy density (up to 6.00 J cm<sup>-2</sup>), and pulse frequency (5 or 500 Hz), we found that R or NIR irradiations can be helpful to promote cell proliferation. Many in vitro and in vivo studies have shown that red (600–700 nm) or NIR (770-1200 nm) spectrums have positive effects on cell

www.adv-biosys.com

growth,[37] differentiation,[38] and anti-inflammation,[39] which is in line with our observation. It is mainly due to the fact that light with longer wavelength causes less absorption and scattering of light into the tissue than the light with shorter wavelength (e.g., blue or green). There are many reports regarding the biphasic dose-response in PBM therapy showing that the PBM effect can be positive or negative to cell viability, depending on the energy density or irradiation time. [40-43] In this study, the half duty cycle was applied to 5 or 500 Hz, thereby lowering the energy densities at 5 or 500 Hz by approximately 50% compared to the energy density of CW. However, the pulse frequency experiment showed unexpected data that R-PW500 irradiation significantly reduced the cell viability (vs R-CW or R-PW5). In addition, the efficacy of NIR-PW500 on anti-inflammation was significantly lower than that of NIR-CW or NIR-PW5, indicating high pulse frequency could be detrimental to cell proliferation, particularly under inflammatory condition. Although we observed energydependent efficacies (biphasic dose-response) on R-PW500 irradiation (peak at 0.25 J cm<sup>-2</sup>, Figure 5A), PW<sub>5</sub> and PW<sub>500</sub> irradiations (either R or NIR) exhibited significantly different efficacies at same energy densities. In spite of the same energy density under different pulsed frequencies (i.e., PW5 vs PW<sub>500</sub>), cellular energy status (i.e., ATP level) could be different due to delayed luminescence that is the prolonged ultraweak luminescence emitted by the biological system after the light source is switched off.<sup>[44-46]</sup> As the negative effect was mainly observed under LPS stimulus in this study, it is speculated that cell inflammation may affect cellular energy status under high-frequency irradiance, thereby exhibiting negative effects. It is also possible that high-frequency irradiation may overstimulate mitochondrial cytochrome c oxidase that acts as a photoacceptor and photosignal transducer, [47] or causes the release of cytochrome c from mitochondria due to the collapse of the  $\Delta\Psi$ m,<sup>[48]</sup> resulting in subsequent cell death. In our study, a high PW frequency stimulus negatively affects the cell viability under LPS stimulus even at lesser energy density than CW (under the same exposure time), which is an opposite trend from the previous report, suggesting further investigation on the role of PW frequency.

When a pathogen infects a host cell, the cell releases ROS and cytokines to recognize and remove foreign molecules such as LPS and to recruit immune cells.<sup>[9]</sup> While intracellular ROS helps to eliminate pathogens and foreign molecules, certain microbial consortiums often induce excessive ROS, resulting in irreparable levels of tissue damage in the host.[49,50] Under the optimal PBM condition, either R or NIR effectively inhibited LPS-induced inflammation and ROS production. It has been reported that there are some potential signaling pathways involved in LPS-induced cell inflammation. For example, once LPS binds to TLR4, the level of MyD88 expression is increased, thereby it phosphorylates NF- $\kappa$ B.<sup>[9]</sup> Recently, it has been also reported that Nox4 can interact directly with the cytoplasmic tail of TLR4.[11] The Nox4 protein can transfer electrons from NADPH to O2 to produce O2.-, and these peroxide free radicals rapidly convert H2O to H2O2 and O2 in the cell to generate intracellular ROS.[12] Intracellularly produced ROS then induces NF-kB activation and its activation increases the transcription of genes involved in innate immune and inflammatory responses.[14] Our data revealed that PBM therapy did not significantly affect the expression level of TLR4 but significantly reduced the expression level of Nox4 and its downstream signaling (MyD88, TRAF6, p-TAK1, p-IKK $\alpha/\beta$ , p-I $\kappa$ B $\alpha$ , and p-NF- $\kappa$ B; Figure 4E,F). Therefore, it seems that the major inhibition pathway of anti-inflammation by R or NIR irradiation is through Nox4-MyD88-NF-κB in this model (see Figure S4, Supporting Information). It has been reported that ionizing radiation or blue light (405 nm) irradiation exhibited enhancement of Nox4 expression level and ROS production, while those induced ROS productions could be diminished by inhibiting Nox4 expression level genetically or pharmacologically.[51,52] Our data showed that the production of ROS can be regulated by R or NIR irradiation without using any drugs, indicating a potent of PBM therapy as a Nox4 regulator.

Meanwhile, B irradiation reduced cell viability significantly compared to control in our study. Indeed, blue (380-500 nm) spectrums were widely used to kill a pathogen. For example, blue light therapy is a clinically accepted approach for *Propioni*bacterium acnes infections.<sup>[53]</sup> Also, studies on blue light inactivation of important wound pathogenic bacteria, including Staphylococcus aureus, [54] P. aeruginosa, [55] and Candida albicans<sup>[56]</sup> have also been reported. Moreover, clinical trials have been conducted to investigate the use of blue light for the treatment of stomach infection by Helicobacter pylori, which was promising.[57] Since NIR irradiation exhibited outstanding efficacy of protecting cell viability and recovering from inflammation, it may be interesting to test a mixed B/NIR irradiations to improve the efficacy of PBM therapy that may result in killing pathogenic bacteria without negatively affecting the viability of host.

It is noteworthy that as the A549 cells were derived from human lung cancer, it may have different mitochondrial structures and metabolism from normal cells, thereby possibly resulting in different responses to light irradiation. Furthermore, chromophores in human epithelium could be different under irradiation by different wavelengths in the same color (e.g., 400–425 vs 465 nm in blue LEDs), thus the use of different wavelengths of each colored LED may cause different cell responses. Therefore, the response of a specific cell to PBM therapy should be comprehensively tested before clinical trial to maximize therapeutic efficacy and to avoid potential harmful effects.

#### 4. Conclusion

Collectively, we demonstrated the comprehensive analysis of the efficacy of PBM therapy in the LPS-A549 model depending on wavelength, irradiation time, and pulse frequency using a custom-built near-contact LED platform. These results suggest that applying PBM therapy with optimal energy density and pulse frequency is critical to prevent cell inflammation or to treat inflamed cells by bacterial invasion since PBM therapy could either beneficial or detrimental to the host. The data may have important ramifications beyond the A549-LPS model, as PBM therapy may be applied to other human body compartments impacted by bacterially induced inflammation.

www.adv-biosys.com

## 5. Experimental Section

LED Disc: Four LEDs with different wavelengths were selected: Blue (B)  $\lambda=465$  nm (445–487 nm; APTD1608VBC/D, Wurth Electronics, Inc., Germany); Green (G)  $\lambda=575$  nm (545–605 nm; SM0402GC, Bivar, Irvine, CA); Red (R)  $\lambda=615$  nm (610–620 nm; SML-P12U2TT86R, ROHM Semiconductor, UK); and NIR  $\lambda=880$  nm (830–930 nm; APT2012SF4C-PRV, Kingbright, City of Industry, CA). The miniaturized LED platform was fabricated by connecting a resistor in series with an LED (1.2 kΩ for red, green, and blue LEDs and 220 Ω for NIR LED) to limit the current to protect electronics. After the LED circuit was assembled on a printed circuit board (PCB), it was placed in a slot of the 3D printed disc, followed by subsequent electrical and thermal passivation by 3D printing resin. Using insulated wires (29 AWG), the LED circuit could be connected to an external LED driving circuitry (pulse frequency PBM therapy) or a power supply directly.

Cell Culture and Cell Viability Assay: Human alveolar basal epithelial (A549; CCL-185, ATCC) cells were cultured in Kaighn's modification of Ham's F-12 medium (F-12K medium; 10-025-CV, Corning, Costar, NY) containing 10% v/v fetal bovine serum (FBS; 16140071, Gibco, Belgium) and 100 U mL<sup>-1</sup> Antibiotic-Antimycotic (15240096, Gibco) at 37 °C in a humid atmosphere of 5% CO<sub>2</sub>. Initially, A549 cells were seeded at  $1 \times 10^4$  cells per well in 24-well plate and grown for 24 h at 37 °C. After 24 h of incubation, cells were washed with 1× phosphatebuffered saline (PBS) and incubated in medium without FBS for an additional 24 h after relevant treatments (LED irradiation and/or LPS treatment). Cell viability was determined at 0, 12, 24, and 48 h using (3-(4,5-dimethylthiazol-2-yl)-2,5-diphenyltetrazolium bromide) (MTT; cell proliferation kit I, Roche, Germany) as described elsewhere.<sup>[58]</sup> Briefly, 50 µL of the MTT labeling reagent (final concentration of 0.5 mg mL<sup>-1</sup>) was added to each well. Then, the cells were incubated in a CO<sub>2</sub> incubator at 37 °C for 4 h. A total of 500 µL of the solubilization buffer (10% SDS in 0.01 M HCl) was added and the plate was allowed to stand overnight in the incubator to solubilize the formazan crystals. The optical density (OD) values of samples were then measured at a wavelength of 570 nm with a microplate reader (BioTek, Winooski, VT). OD values of the treatment groups were always normalized to that of the untreated control group.

PBM Therapy on Epithelial Cell: To test the efficacy of PBM therapy, A549 cells were seeded at  $1\times10^4$  cells per well in 24-well plate and grown for 24 h at 37 °C. After 24 h, the cells were washed and the culture medium was replaced as described in the previous section. Then, the cells were placed on the LED platforms to be exposed to each wavelength of LED for various times (up to  $\approx\!6$  J cm $^{-2}$ ) (see LED platform and Table S1, Supporting Information, for detail). To test the effect of pulse frequency, we also used low (5 Hz) or high (500 Hz) pulse frequencies of R or NIR for a range of energy density (up to  $\approx\!3$  J cm $^{-2}$ ). After PBM therapy, the cells were incubated for an additional 24 h and the viability was determined as described in the previous section.

Cell Inflammation by Bacterial LPS: To investigate the cell response to bacterially induced inflammation, we exposed the cells to LPS (L9143, Sigma, St. Louis, MO). First, we determined the optimal concentration of LPS for inflammation induction by adding various concentrations of LPS (0–100  $\mu g \ mL^{-1}$ ). After A549 cells were grown for 24 h, the cells were washed and the culture medium was replaced with fresh media (0% FBS). Then, LPS was added and the cells were subsequently incubated for an additional 24 h. With a predetermined optimal concentration of LPS (0–20  $\mu g \ mL^{-1}$ ), we also pretreated the cells with LEDs before LPS exposure as described in the previous section on PBM therapy, and the cells were subsequently incubated for an additional 24 h. Then, the viability of cells was evaluated using MTT assay (see section Cell Culture and Cell Viability Assay for detail).

Enzyme-Linked Immunoassay for Inflammation Markers (IL-6 and TNF- $\alpha$ ): The level of inflammation markers (IL-6 and TNF- $\alpha$ ) of the supernatant of various concentrations of LPS-treated (0–100  $\mu$ g mL<sup>-1</sup>) cells was determined using ELISA kits (205991004 for IL-6 and 201629004 for TNF- $\alpha$ , Invitrogen, Rockford, IL) according to the manufacturer's

protocol. [59] Then, the level of IL-6 and TNF- $\alpha$  of the supernatant of LPS-treated (20  $\mu$ g mL<sup>-1</sup>) cells in the absence/presence of R and NIR irradiation was also determined. Absorbance for IL-6 and TNF- $\alpha$  was measured at 450 nm using a colorimetric microplate reader.

ROS Detection with  $H_2DCF$ -DA Assay: The production of ROS was visualized by using 2′,7′-dichlorodihydrofluorescein diacetate ( $H_2DCF$ -DA; Sigma) and quantified using ImageJ. <sup>[60]</sup> After the cell inflammation experiment using various concentrations of LPS (0–100  $\mu g$  mL<sup>-1</sup>), each condition was subjected to the ROS assay. This assay was also performed to the LPS-treated (20  $\mu g$  mL<sup>-1</sup>) cells in the absence/presence of R and NIR irradiation. To visualize the produced ROS, the A549 cells were incubated with 1  $\mu$ M of DCF-DA for 45 min at 37 °C. After DCF-DA incubation, cells were washed with PBS and DCF fluorescence intensity was monitored using a fluorescence microscope (Olympus, IX71, Japan) with excitation at 485 nm and emission at 530 nm, respectively.

Quantitative Real-Time PCR: After the PBM therapy on LPS-treated A549 cells, the cells were collected and total RNA was isolated with RNeasy Mini kit (Qiagen, Valencia, CA) for qRT-PCR. [61] To synthesize cDNA from total RNA, iScript Reverse Transcription Supermix (Bio-Rad Laboratories, Hercules, CA) was used according to the manufacturer's protocol. Gene-specific RT-PCR primers were selected from the mRNA sequences obtained from NCBI's reference sequence database (http://www.ncbi.nlm.nih.gov/refseq/). The primer sets for quantitative real-time PCR were follows: TLR4: 5'-GAGTCCACTGGCGTCTTCAC-3' (forward) and 5'-ATGACGAACATGGGGGCATC-3' (reverse); MyD88: 5'-GTTTGTCAGGAGAGATGATCC-3' (forward) and 5'-CTCCTGGTTCTCCTGCTTGG-3' (reverse); and GAPDH: 5'-GAGTCCACTGGCGTCTTCAC-3' (forward) and 5'-CTCCTGGTTCTCCTGCTTGG-3' (reverse); and GAPDH: 5'-GAGTCCACTGGCGTCTTCAC-3' (forward) and 5'-ATGACGAACATGGGGGCATC-3' (reverse).

Cells Western Blotting: were lvsed radioimmunoprecipitation assay buffer (Thermo Fisher Scientific, Rockford, IL) containing protease inhibitor cocktail (P8340, Sigma, St. Louis, MO). The whole-cell lysates (100 µg per lane) were separated by SDS-PAGE and detected with primary antibodies. Primary antibodies specific for TRAF6, p-TAK1, p-IKK $\alpha/\beta$ , p-I $\kappa$ B $\alpha$ , NF-kB, p-NF-kB, and glyceraldehyde 3-phosphate dehydrogenase (GAPDH) were purchased from Cell Signaling Technology (Beverly, MA). Antibodies for TLR4 and MyD88 were obtained from Santa Cruz Biotechnology (Santa Cruz, CA). Antibody for NOX4 was obtained from Novus (St. Charles, MO). The secondary antibodies used were an anti-rabbit IgG, and anti-mouse IgG from Santa Cruz Biotechnology. Bound secondary antibodies were detected using SuperSignal West Pico Chemiluminescent Substrate (Thermo Fisher Scientific). Equal loading was assessed using anti-GAPDH antibody to normalize the amounts of total protein.[62] The protein levels were determined by ImageJ software.

Assessment of ΔΨm: ΔΨm was measured using a MitoProbe JC-1 Assay Kit (Thermo Fisher Scientific). [63] Briefly, trypsinethylenediaminetetraacetic acid-treated cells (1  $\times$  106 cells mL $^{-1}$ ) were incubated in the dark at 37 °C for 15 min in 500 μL of 40 nM JC-1. Data were analyzed using a flow cytometer (BD Biosciences, Santa Clara, CA). Green and red fluorescence were measured at 514/529 nm (FL-1) and 585/590 nm (FL-2), respectively. Cells were kept on ice before analysis. Control experiments were performed in the presence of 50 μM CCCP, an uncoupling agent that can abolish  $\Delta\Psi m$ .

Statistical Analysis: The results from independent experiments were expressed as mean  $\pm$  standard deviation. Statistical analysis of all the experimental data was performed using the Student's t-test with Microsoft Excel. All the experiments were repeated at least four times. Data were considered statistically significant when p-value is less than 0.05.

## **Supporting Information**

Supporting Information is available from the Wiley Online Library or from the author.

www.adv-biosys.com

## Acknowledgements

This work was partially supported by University of Pennsylvania start-up funds (G.H.) and Temple University start-up funds (A.K.).

## **Conflict of Interest**

The authors declare no conflict of interest.

### Keywords

host-bacteria interaction, inflammation, light-emitting-diode, photo-biomodulation, reactive oxygen species

Received: September 19, 2019 Revised: December 9, 2019 Published online:

- L. Eckmann, M. F. Kagnoff, J. Fierer, Infect. Immun. 1993, 61, 4569.
- [2] D. Heumann, T. Roger, Clin. Chim. Acta 2002, 323, 59.
- [3] Z. Xu, D. Dong, X. Chen, H. Huang, S. Wen, Biomed. Res. Int. 2015, 2015, 849475.
- [4] M. S. Byrd, B. Pang, M. Mishra, W. E. Swords, D. J. Wozniak, mBio 2010, 1, 140.
- [5] J. K. Ichikawa, A. Norris, M. G. Bangera, G. K. Geiss, A. B. van't Wout, R. E. Bumgarner, S. Lory, Proc. Natl. Acad. Sci. USA 2000, 97, 9659
- [6] T. Wu, S. Chan, C. Chang, P. Yu, C. Chuang, S. Yeh, Chem.-Biol. Interact. 2018, 292, 101.
- [7] E. K. Benedikz, D. Bailey, C. N. Cook, D. Gonçalves-Carneiro, M. M. Buckner, J. M. Blair, T. J. Wells, N. F. Fletcher, M. Goodall, A. Flores-Langarica, Sci. Rep. 2019, 9, 7903.
- [8] C. V. Rosadini, J. C. Kagan, Curr. Opin. Immunol. 2017, 44, 14.
- [9] A. He, R. Ji, J. Shao, C. He, M. Jin, Y. Xu, Inflammation 2016, 39, 172.
- [10] H. S. Park, H. Y. Jung, E. Y. Park, J. Kim, W. J. Lee, Y. S. Bae, J. Immunol. 2004, 173, 3589.
- [11] M. Lu, Q. Zhang, K. Chen, W. Xu, X. Xiang, S. Xia, Phytomedicine 2017, 36, 153.
- [12] T. Lawrence, Cold Spring Harb. Perspect. Biol. 2009, 1, a001651.
- [13] M. R. Hamblin, AIMS Biophys. 2017, 4, 337.
- [14] R. J. Lanzafame, I. Stadler, A. F. Kurtz, R. Connelly, P. Brondon, D. Olson, Lasers Surg. Med. 2007, 39, 534.
- [15] Q. Wu, W. Xuan, T. Ando, T. Xu, L. Huang, Y. Huang, T. Dai, S. Dhital, S. K. Sharma, M. J. Whalen, *Lasers Surg. Med.* 2012, 44, 218
- [16] J. Liebmann, M. Born, V. Kolb-Bachofen, J. Invest. Dermatol. 2010, 130, 259.
- [17] Q. Sun, H. Kim, H. Cho, S. Shi, B. Kim, O. Kim, J. Photochem. Photobiol., B 2018, 186, 31.
- [18] Y. Hsu, Y. Lin, C. Chen, Y. Chiu, H. Chiu, J. Mol. Med. 2017, 95, 1203.
- [19] B. Tran, S. R. Feldman, J. Dermatol. Treat. 2011, 22, 18.
- [20] V. S. Grandinétti, E. F. Miranda, D. S. Johnson, P. R. V. de Paiva, S. S. Tomazoni, A. A. Vanin, G. M. Albuquerque-Pontes, L. Frigo, R. L. Marcos, P. T. C. de Carvalho, E. C. P. Leal-Junior, *Lasers Med. Sci.* 2015, 30, 1575.
- [21] J. A. Keelan, M. Blumenstein, R. Helliwell, T. A. Sato, K. W. Marvin, M. D. Mitchell, *Placenta* 2003, 24, S33.
- [22] H. Hsu, M. Wen, J. Biol. Chem. 2002, 277, 22131.

- [23] A. V. Kuznetsov, I. Kehrer, A. V. Kozlov, M. Haller, H. Redl, M. Hermann, M. Grimm, J. Troppmair, Anal. Bioanal. Chem. 2011, 400, 2383.
- [24] H. S. Park, J. N. Chun, H. Y. Jung, C. Choi, Y. S. Bae, Cardiovasc. Res. 2006, 72, 447.
- [25] A. Singh, B. Koduru, C. Carlisle, H. Akhter, R. Liu, K. Schroder, R. P. Brandes, D. M. Ojcius, Sci. Rep. 2017, 7, 14346.
- [26] G. K. Keshri, A. Gupta, A. Yadav, S. K. Sharma, S. B. Singh, PLoS One 2016, 11, e0166705.
- [27] T. Ando, W. Xuan, T. Xu, T. Dai, S. K. Sharma, G. B. Kharkwal, Y. Huang, Q. Wu, M. J. Whalen, S. Sato, *PLoS One* **2011**, 6, e26212.
- [28] A. Mostafavinia, R. M. Farahani, M. Abbasian, M. V. Farahani, M. Fridoni, S. Zandpazandi, S. K. Ghoreishi, M. A. Abdollahifar, R. Pouriran, M. Bayat, *Iran Red Crescent Med. J.* 2015, 17, e29513
- [29] J. D. Ly, D. R. Grubb, A. Lawen, Apoptosis 2003, 8, 115.
- [30] M. T. Binet, C. J. Doyle, J. E. Williamson, P. Schlegel, J. Exp. Mar. Biol. Ecol. 2014, 452, 91.
- [31] K. Kwon, B. Viollet, O. J. Yoo, Biochem. Biophys. Res. Commun. 2011, 416. 343.
- [32] A. P. Sommer, A. L. Pinheiro, A. R. Mester, R. Franke, H. T. Whelan, J. Clin. Laser Med. Surg. 2001, 19, 29.
- [33] J. P. da Silva, M. A. da Silva, A. P. F. Almeida, I. L. Junior, A. P. Matos, *Photomed. Laser Surg.* 2010, 28, 17.
- [34] J. J. Anders, R. J. Lanzafame, P. R. Arany, Photomed. Laser Surg. 2015, 33, 183.
- [35] L. F. de Freitas, M. R. Hamblin, IEEE J. Sel. Top. Quantum Electron. 2016, 22, 348.
- [36] T. Karu, Photomed. Laser Surg. 2010, 28, 159.
- [37] P. Moore, T. D. Ridgway, R. G. Higbee, E. W. Howard, M. D. Lucroy, Lasers Surg. Med. 2005, 36, 8.
- [38] W. Li, Y. Leu, J. Wu, Photomed. Laser Surg. 2010, 28, 703.
- [39] F. Aimbire, R. Albertini, M. Pacheco, H. C. Castro-Faria-Neto, P. Leonardo, V. V. Iversen, R. Lopes-Martins, J. M. Bjordal, *Photomed. Laser Surg.* 2006, 24, 33.
- [40] Y. Wang, Y. Huang, Y. Wang, P. Lyu, M. R. Hamblin, Biochim. Biophys. Acta, Gen. Subj. 2017, 1861, 441.
- [41] I. Jaadane, G. E. Villalpando Rodriguez, P. Boulenguez, S. Chahory, S. Carré, M. Savoldelli, L. Jonet, F. Behar-Cohen, C. Martinsons, A. Torriglia, J. Cell. Mol. Med. 2017, 21, 3453.
- [42] S. K. Sharma, G. B. Kharkwal, M. Sajo, Y. Huang, L. De Taboada, T. McCarthy, M. R. Hamblin, Lasers Surg. Med. 2011, 43, 851.
- [43] Y. Y. Huang, S. K. Sharma, J. Carroll, M. R. Hamblin, Dose Response 2011, 9, 602.
- [44] H. B. Kim, K. Y. Baik, P. Choung, J. H. Chung, Sci. Rep. 2017, 7, 15927
- [45] F. Musumeci, L. A. Applegate, G. Privitera, A. Scordino, S. Tudisco, H. J. Niggli, J. Photochem. Photobiol., B 2005, 79, 93.
- [46] R. Duan, T.C. Liu, Y. Li, H. Guo, L.B. Yao, Lasers Surg. Med. 2001, 29, 174
- [47] T. I. Karu, IUBMB Life 2010, 62, 607.
- [48] N. J. Waterhouse, J. C. Goldstein, O. Von Ahsen, M. Schuler, D. D. Newmeyer, D. R. Green, J. Cell Biol. 2001, 153, 319.
- [49] J. A. Smith, J. Leukocyte Biol. 1994, 56, 672.
- [50] R. Noubade, K. Wong, N. Ota, S. Rutz, C. Eidenschenk, P. A. Valdez, J. Ding, I. Peng, A. Sebrell, P. Caplazi, *Nature* 2014, 509, 235.
- [51] Y. Sakai, T. Yamamori, Y. Yoshikawa, T. Bo, M. Suzuki, K. Yamamoto, T. Ago, O. Inanami, Free Radical Res. 2018, 52, 92.
- [52] C. Roehlecke, U. Schumann, M. Ader, C. Brunssen, S. Bramke, H. Morawietz, R. H. Funk, PLoS One 2013, 8, e71570.
- [53] T. Dai, A. Gupta, C. K. Murray, M. S. Vrahas, G. P. Tegos, M. R. Hamblin, *Drug Resist. Updates* **2012**, *15*, 223.
- [54] C. S. Enwemeka, D. Williams, S. K. Enwemeka, S. Hollosi, D. Yens, Photomed. Laser Surg. 2009, 27, 221.





- [59] Y. T. Zhuang, D. Y. Xu, G. Y. Wang, J. L. Sun, Y. Huang, S. Z. Wang,
- Eur. Rev. Med. Pharmacol. Sci. 2017, 21, 302.
  [60] A. Cossarizza, R. Ferraresi, L. Troiano, E. Roat, L. Gibellini,
  L. Bertoncelli, M. Nasi, M. Pinti, Nat. Protoc. 2009, 4, 1790.
  - [61] T. Nolan, R. E. Hands, S. A. Bustin, Nat. Protoc. 2006, 1, 1559
- [62] B. T. Kurien, R. H. Scofield, in Western Blotting, Vol. 1312 (Eds: B. T. Kurien, R. H. Scofield), Springer, New York, NY 2015, Ch. 5.
- [63] L. Troiano, R. Ferraresi, E. Lugli, E. Nemes, E. Roat, M. Nasi, M. Pinti, A. Cossarizza, Nat. Protoc. 2007, 2, 2719.
- M. E. Sherwood, G. P. Tegos, M. R. Hamblin, Antimicrob. Agents Chemother. 2013, 57, 1238.
  [56] E. G. de Oliveira Mima, A. C. Pavarina, L. N. Dovigo, C. E. Vergani,

[55] T. Dai, A. Gupta, Y. Huang, R. Yin, C. K. Murray, M. S. Vrahas,

- C. A. de Souza Costa, C. Kurachi, V. S. Bagnato, Oral Surg. Oral Med. Oral Pathol. Oral Radiol. Endod. 2010, 109, 392.
- [57] M. R. Hamblin, J. Viveiros, C. Yang, A. Ahmadi, R. A. Ganz, M. J. Tolkoff, Antimicrob. Agents Chemother. 2005, 49, 2822.
- [58] B. Relja, F. Meder, K. Wilhelm, D. Henrich, I. Marzi, M. Lehnert, Int. J. Mol. Med. 2010, 26, 735.